Measurement 46 (2013) 4145–4151

Contents lists available at ScienceDirect

Measurement

journal homepage: www.elsevier.com/locate/measurement

A flexible thin-film for powering stand alone electronic devices

João Paulo Carmo *, José Miguel Gomes, Luis Miguel Gonçalves, José Higino Correia

University of Minho, Dept. of Industrial Electronics, Campus Azurem, 4800-058 Guimaraes, Portugal

ARTICLE INFO

Article history:
Received 21 February 2013
Received in revised form 26 June 2013
Accepted 6 August 2013
Available online 20 August 2013

Keywords:
Flexible sensing system
Flexible film
Flexible bendable energy harvesting system

ABSTRACT

This paper presents a flexible thin-film (FTF) composed by a photovoltaic (PV) cell, a flexible solid-state rechargeable battery and power management electronics. A flexible printed circuit board (fPCB) was used for providing physical support to the electronics and to the battery, whereas a PDMS (polydimethylsiloxane) layer was used for providing mechanical adhesion between the PV cell and the fPCB. The high elasticity of the PDMS makes this material an excellent candidate for adapting two materials with different thermal expansions (fPCB and PV). The physical measurements showed a prototype with a thickness in the range 1.52 ± 0.10 mm, 10 g of weight and 37 × 114 mm of size. The electrical measurements showed ability to provide an output voltage of 3.8 V in a continuously form under these conditions: the PV providing DC power for solar irradiations higher than 6 W m^{-2}, and the battery providing DC power for solar irradiations above bellow 6 W m^{-2} (value that has emerged during the twilight between sunset and dusk).

1. Introduction

In the present days, the deformation of materials (e.g. where any form of bending is present) is still the most used physical principle on transduction [1–12]. There is an increased interest to use this transduction mechanism on a new class of applications with flexible substrates and materials. Such applications include rollable displays, conformable sensors, biodegradable electronics, wearable health monitoring systems, medical implants and other ones with unconventional form factors [13–15]. The relative weak nature of the van der Waals force on intermolecular bonding is the main reason behind the flexibility of flexible materials [16]. The silicon is one of such unsuitable materials because it is simultaneously brittle, cannot be deformed beyond a very short amount and is too heavy, especially on large area devices (such as displays, electronic circuit carriers) [17]. Therefore and contrary to silicon substrates, the flexible materials can obey to a stringent set of specifications in order to comply with high security standards and at the same time be used without limitations where the weight is an important issue [18]. The polydimethylsiloxane (PDMS) is a silicone rubber, which was previously successfully used in the fabrication of flexible stretchable electronic devices [19–22] and for this reason a special attention is given in this paper. Additionally, it is well known that typical electronic devices require batteries, which have limitations in terms of lifetime and capacity [23]. Therefore, incorporating together with the battery some kind of energy retrieving system in the devices is a highly promising solution to the problem [24]. It must be noted that these hybrid devices (composed of energy storage systems and energy scavengers) require an energy management system [25]. The research of flexible devices for powering stand-alone microsystems constitutes an emergent field with few prototypes already available, whose grown is expected for the next years [26,27]. One of the most important renewable energy sources are those based on photovoltaic (PV) cells [28–31] because their technology is well established in terms of maturity, applications and markets. Therefore and taking all of this into account, this paper presents a flexible thin-film (FTF) comprising a photovoltaic (PV) cell, a flexible rechargeable battery and power management electronics. The proposed FTF is highly flexible because of

* Corresponding author. Tel.: +351 253510190; fax: +351 253510189.
E-mail address: jcarmo@dei.uminho.pt (J.P. Carmo).

0263-2241/$ - see front matter © 2013 Elsevier Ltd. All rights reserved.
http://dx.doi.org/10.1016/j.measurement.2013.08.016

the PDMS structure used to join the PV cell into the flexible printed circuit board (fPCB) with power management electronics. A FTF prototype was built and tested.

2. Design and fabrication

2.1. FTF concept

Fig. 1 illustrates the flexible substrates forming the FTF (PV cell, fPCB and PDMS as a key-element – e.g. as the adhesion layer) and the respective constructive concept.

The Fig. 2 shows the block diagram of the FTF, which is composed by the PV cell, a DC–DC converter, a lithium polymer battery and the respective protection circuit. As discussed further, the energy management system uses the DC–DC converter with the battery protection circuit.

2.2. FTF design

The materials were selected in order to fabricate a FTF with enough flexibility for fixing into curved surfaces and suitable enough to provide power to electronic devices. These targets were reached by carefully selecting a PV cell made of thin-films, a flexible rechargeable battery, a flexible PCB, integrated circuits (ICs) with reduced profile (e.g. surface mount devices, SMDs) and a flexible material for adhesion.

The PDMS was selected as adhesion substrate due to their unique electromechanical properties: it behaves as a thermo-rigid material with high elasticity, high resistance to the heat and to the flame; it is physically inert; it presents good dielectric properties, high resistance to aging, resistance to the degradation caused by the UV exposition, as well as, a naturally hydrophobic surface [32,33]. Moreover, the PDMS acts as mechanical buffer for absorbing the majority of deformations. The flexibility and the elasticity of this material remain constant within a large temperatures range, e.g. from −45 to 200 °C. Moreover, the PDMS presents a low-cost of fabrication [34]. The PDMS can be acquired as a kit with these two parts: a polymer and a hardener agent [35]. The former is known as base agent, while the later is known as cura's agent, being both available in the liquid phase. These two agents must obey to a 1:10 proportion, more precisely only one part of cure's agent must be mixed into ten parts of base agent.

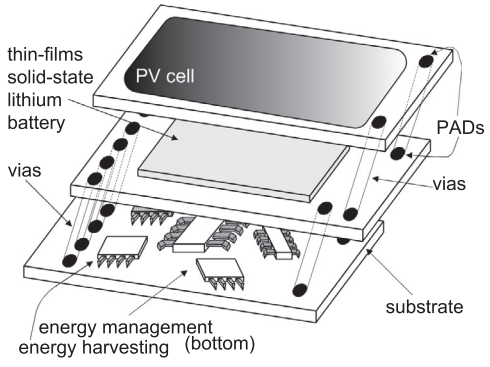

Fig. 1. Autonomous flexible thin-film (FTF) concept.

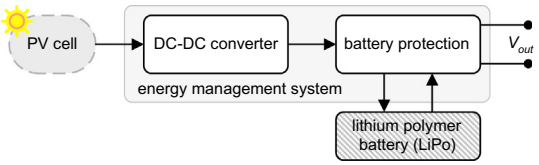

Fig. 2. Block diagram of the FTF.

A thermal treatment can be used simultaneously in the next step for reducing the time required for curing. The change from the liquid into the solid phase can takes at least 48 h, when performed at the room temperature [32]. Additionally, this time can be reduced downwards to 2 h at temperatures of 80 °C [35]. Young's Modulus E_{PDMS} (measured as the relation between the applied force and the material's elasticity) of the PDMS depends on the proportion between the cure's agent and the base agent. Typical values of E_{PDMS} vary from 12.5 kPa to 4 MPa. It was used the PDMS Sylgard 184 from the manufacturer *Dow Corning* [32].

It was selected the flexible fPCB Pyralux from the manufacturer DuPont, which is constituted by three layers [36]. The first layer is the substrate and is constituted by polyimide.

This material is a highly flexible polymer with a high resistance to high temperatures during long periods of time. The thickness of this first layer can vary typically between 25 and 127 μm. The second layer is constituted by an acrylic adhesive with a thickness in the range 13–51 μm. This is an adaptation layer for gluing the first into the third conductive layer. The third layer is constituted by copper, whose quantities can be found within the range 153–610 g m^{-2}. The high thermal stability was another reason behind the selection of this fPCB.

The battery selected for the FTF prototype was the PowerStream's model PGEB0054338, measuring 43 mm × 38 mm with a thickness of only 0.6 mm. This is a flexible lithium polymer rechargeable with a capacity of 45 mAh and with a nominal voltage of 3.7 V [37]. The manufacturer recommends the working voltage to be within the range 2.8–4.2 V.

The PV cell model MP3-37 from the manufacturer Powerfilm Solar occupies an area of 42.18 cm^2 (measuring 114 mm × 37 mm) and under the maximum solar irradiation, can provide a maximum output power of 0.15 W with 3 V and a current of 50 mA [38].

The power management electronics is composed by a DC–DC step-up converter (to provide a regulated voltage both for recharging the battery and for external supply) and by a circuit to manage the battery charge/discharge (e.g. for protecting the battery) [39]. The Linear Technology's LTC3105 is a microdevice specific for low-power applications, which incorporates internally a user-adjusted control for Maximum Power Point Tracking (MPPT). This makes easy the use of energy sources with high impedances, such as PV cells. The output voltage can be adjusted and keeping efficiency above 90%, proving also thermal protection. The Linear Technology's LTC4071 is responsible for managing the charge/discharge of the battery. In fact,

this microdevice protects the battery from overvoltage peaks that can occur during the battery's charge, as well as from undervoltage valleys that can occur during the battery's discharge, disconnecting the battery from the charge/discharge circuit. The complete circuit is illustrated in Fig. 3.

2.3. FTF fabrication

The fPCB board was patterned by photolithography. The precision of photolithography was enough for patterning the PCB and simultaneously to keep the PCB fabrication process relatively simple.

The process to patterning the fPCB followed these steps: (a) pattern drawing in the mask, (b) photoresist (PR) layer application above the fPCB surface, (c) PR baking during 15 min and subjected to a temperature of 70 °C, (d) ultraviolet (UV) light exposition during 60–120 s. The transferred pattern into the PR (and into the fPCB) was the mask's pattern because the used PR consisted in the positive 20 [36]. Furthermore, (e) the fPCB was kept immersed during 60 s within a sodium hydroxide (NaOH) solution with a concentration of 10 g for each liter of water. Then, (f) the mask's pattern was transferred into the surface of the fPCB by etching away the unprotected copper on an iron perchloride ($FeCl_3$) solution with a concentration of 400 g per liter of water. After the etching step, (g) acetone was used to strip the PR.

The SMD components that compose the power management electronics were soldered into the fPCB board just after the respective patterning. During the next step, a layer of PDMS has been spread throughout the area containing the whole circuit. The PV cell was further attached, forming the final FTF module. Finally, the final FTF module has been maintained during 2 h in a oven, with temperature constant and equal to 40 °C, allowing the PDMS to stiffen.

Fig. 4 shows photographs of the FTF prototype, measuring a width of 37 mm by a length of 114 mm, presenting a thickness in the range 1.52 ± 0.10 mm, as well as 10 g of weight.

3. Experimental

3.1. Measurement setup

Fig. 5 shows the experimental setup used for doing the optoelectronic measurements of the FTF. As illustrated, the FTF was characterized with the help of the experimental

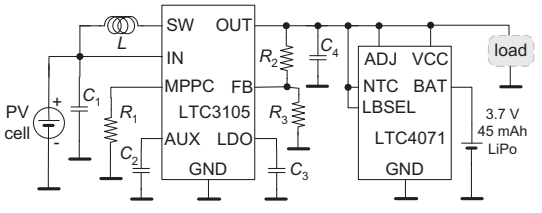

Fig. 3. Electronic circuit, including MPPT step-up conversion, battery power management and under/over voltage protection.

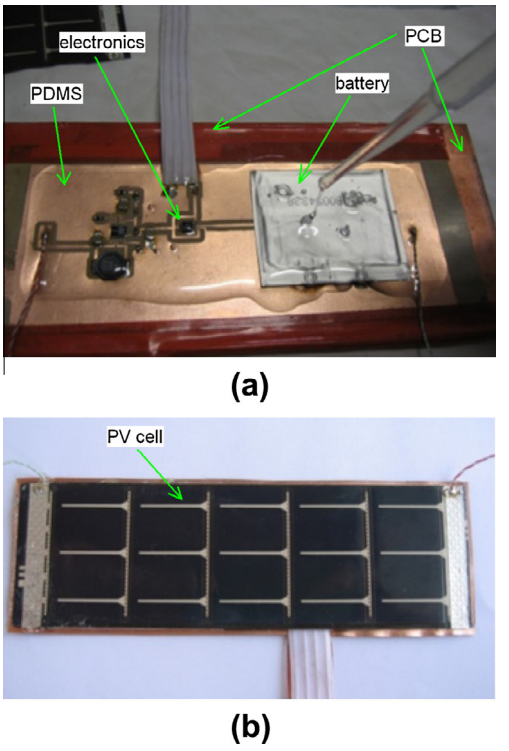

Fig. 4. Photographs of the FTF prototype: (a) just after the PDMS application and (b) after the PV cell placement.

setup composed by a radiometer Delta Ohm model HD2102.1 with an irradiation cell LP471 (able to measure the range 0.1–2000 W m^{-2} and the 400–1050 nm wavelengths) and by a lux-meter TES 1335 (able to measure over the range 0–400000 Lx). The currents and voltages were measured with the help of common multimeters.

3.2. Power and efficiency of the TFT

The Fig. 6 shows the FTF behaviour (power and efficiency) over a clear spring-day measured from the sunrise (at 08:11 AM) up to the sunset (at 17:20 PM), at a latitude of 41°N. Typical electrical efficiency (defined as the ratio

Fig. 5. Photograph showing the optoelectronic measurement setup, where it is possible to observe the luximeter (on left) and the radiometer (on right), whose sensors are positioned in the same plane of the FTF (containing the FTF holder).

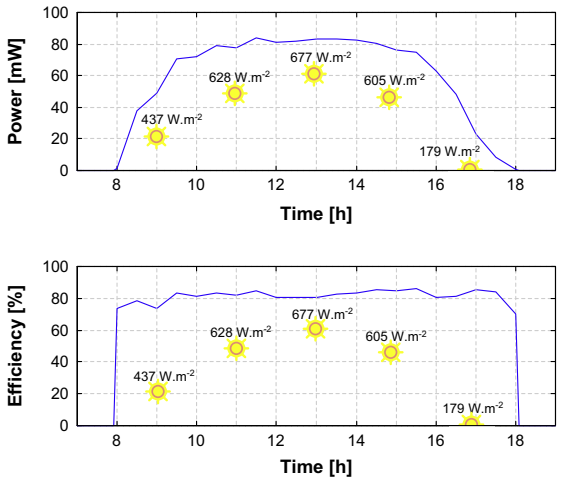

Fig. 6. Power and efficiency of the FTF in a typical clear spring day at latitude of 41°N.

between the charging power of battery to the output power from the PV cell) values are above 80%, for irradiance above 30 W m^{-2}. Power output above 80 mW can be obtained with irradiance above 600 W m^{-2}.

The behaviour of the FTF circuit and PV (with and without series Schottky's diode) was compared during three sets (type) of measurements. The solar irradiation was ramped down and up between 0 and 650 W m^{-2}, and the power delivered to the battery registered in the three circuits (FTF, PV connected to battery, and PV connected to battery trough a diode). The voltage in the terminals of the battery was fixed at 3.8 V before starting each set of measurements. It can be observed in the Fig. 7 that the available power for the same levels of irradiation decreases drastically, even after using a Schottky's diode with a voltage drop of only 0.2 V. For irradiation levels below 300 W m^{-2} the diode became reversely biased, preventing the battery to discharge. For the same conditions, the FTF make available a charge power significantly higher than those available in the remaining cases. In fact, the FTF

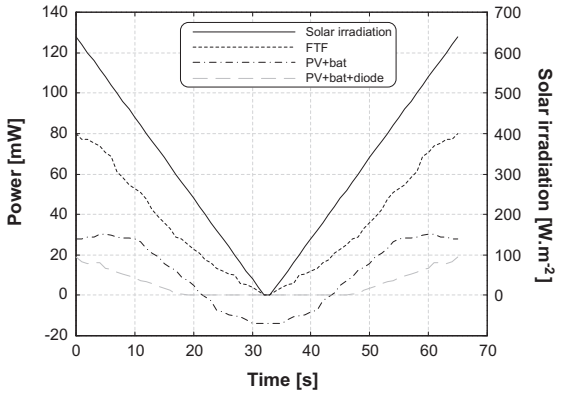

Fig. 7. Comparative of output power of the FTF versus a PV connected to battery (with and without diode).

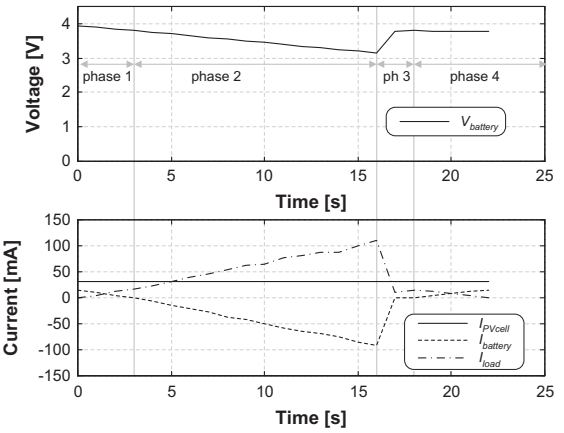

Fig. 8. FTF behaviour when supplying a variable load.

can delivery power to the battery with irradiations below 6 W m^{-2} (between the sunset and the dusk).

3.3. FTF supplying a load

The Fig. 8 shows the dynamical behaviour of the FTF when supplying a variable load purely resistive. The resistance was settled to a high value in the beginning of the phase 1. At this point, the load does not drain current and therefore the PV cell is dedicated to the battery charging. A current fraction from the PV cell begins to flow across the load, when decreasing its resistance. In the end of phase 1 (and starting of the phase 2) all the current from the PV cell flows across the load and at the same time, the battery charging stops. During the phase 2, the current excess drained by the load was provided by the battery. The terminus of the phase 2 masks the beginning of a new phase, with the entering in action of the circuit responsible for protecting the battery from undervoltage valley. This protection circuit makes the load current to decrease, blocking current to be drained from the battery. Then, the resistance load was intentionally increased again in order to force the required power by the load to be smaller than the power able to be provided by the PV cell. This marks the end of the phase 3 and the start of the phase 4, with the PV cell able to simultaneously supply the load and recharge the battery. This last experimental result is important because it proves the suitability of the FTF to

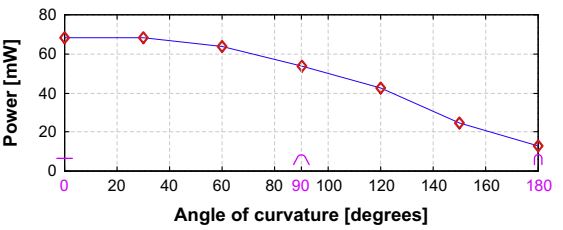

Fig. 9. Power versus the angle of curvatures imposed to the FTF.

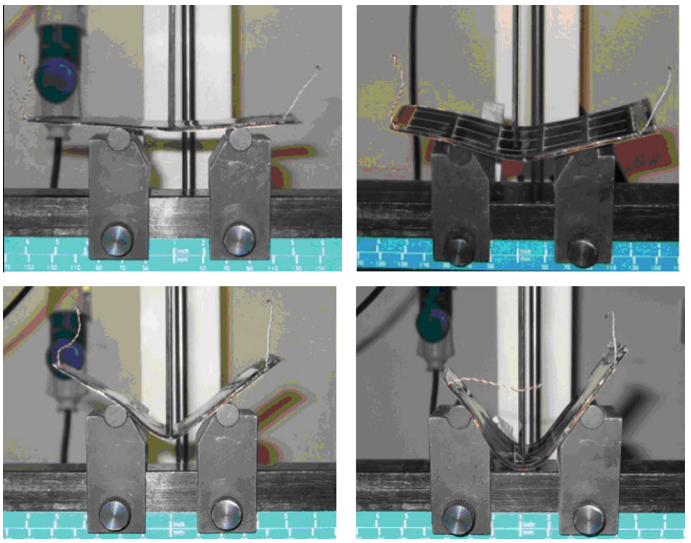

Fig. 10. Progressive bending of the FTF in response to the vertical force.

power stand-alone microdevices without the need of the programmed actions of maintenance by human operators.

3.4. FTF behavior to bending

The power delivered by the FTF is maximum, when the normal direction to the PV cell's surface is oriented towards the sun. It will be expected a reduction in the maximum delivered power by decreasing the angle between the FTF's surface with the sunlight rays. Therefore, it is of great interest to quantify the power reduction with adopted angle. In this context, the Fig. 9 shows the delivered power variations as a function of the angle of curvature imposed to the FTF.

The power delivered by the FTF decreases almost linearly with the angle, starting at 100% with 0° down to 20% with 180°. A close look to the graph allows the identification of two different decrease rates: the first one for angles between 0° and 60° and a second for angles larger than 60°. The rate of decrease (measured in microwatt for each added degree of curvature) in the first part of the graph is 77 μW^{-1}, whereas from 60° and behind is 420 μW^{-1}.

3.5. Mechanical behavior

The mechanical behavior of the FTF was also characterized with the target to test the mechanical resistance and flexibility of the FTF prototype. A set of sixty tests were sequentially done, and consisted in the flexion applied to three points in the FTF. The test setup consisted in the dynamometer model H100KS from the manufacturer Hounsfield.

These tests are done as follows: the target material under evaluation (e.g. the FTF) is supported at two points spaced apart between each other. Then, a vertical force is applied at a third point in the direction from the top towards the bottom. It must be noted that the third point is located in the middle distance between the two points of support previously referred. This can be confirmed in the four photographs showed in Fig. 10. Fig. 10 also shows the sequence under the application of the downward force, whose result is the progressive bending of the FTF. The distance between the two support points is 5 cm and at the same time, the dynamometer was parameterized to provide a maximum displacement of 25 mm with a speed of 25 mm per minute.

The plot on top of Fig. 11 shows the forces and the respective displacements for the first set of five tests, while the results for the 55 remaining tests are showed in the bottom plot of the same figure.

The high forces that result within the first set of five tests showed a brief softening period, in which the FTF presents high rigidness. As showed on top of Fig. 11, this was

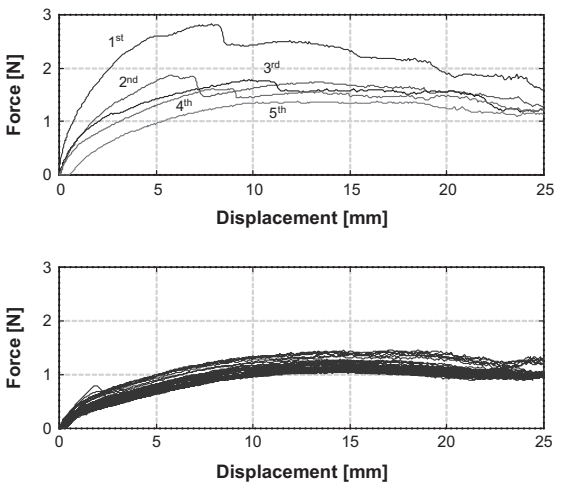

Fig. 11. Applied forces into the FTF and the resulted displacements that were measured in the (top plot) first and (bottom plot) second sets of tests.

the reason to increase the applied force up to about 3 N for bending the FTF. It can also be observed that the followed 55 remaining tests done with the FTF showed a stable and predicted behavior for applied forces up to 1 N.

4. Applications

The high-precision agriculture (HPA) is an emergent field, where the demand for stand-alone devices is growing in the last years [40]. These devices are even more used on in-field acquisition (for example, on pest monitoring, soil chemical content and other weather conditions) and transmitting data towards management centers) and must operate without the need of maintenance for long periods of time [41]. Therefore, the potential of the FTF for use on HPA is huge.

5. Conclusions

This paper presented a flexible thin-film (FTF) for powering stand alone electronic devices. The FTF was easily fabricated using flexible substrates (e.g. PDMS, fPCBs and PV cells) The fabricated FTF was flexible, and therefore, it can successfully installed to provide electrical energy for stand-alone microdevices.

Acknowledgments

This work was fully supported by the Portuguese Foundation for Science and Technology *FlexSolar* project with the reference grant FCT/PTDC/EEA-ELC/114713/2009. We also would like to thanks to Mr. Joaquim Jorge from the Textile Engineering Department (DET) at University of Minho for the help during the mechanical tests with the dynamometer.

References

[1] D.-S. Xu, J.-H. Yin, Z.-Z. Cao, Y.-L. Wang, H.-H. Zhu, H.-F. Pei, A new flexible FBG sensing beam for measuring dynamic lateral displacements of soil in a shaking table, Measurement 46 (1) (2013) 200–209.
[2] Y.C. Lee, T.S. Liu, C.I. Wu, W.Y. Lin, Investigation on residual stress and stress-optical coefficient for flexible electronics by photoelasticity, Measurement 45 (3) (2012) 311–316.
[3] J. Knapp, E. Altmann, J. Niemann, K.-D. Werner, Measurement of shock events by means of strain gauges and accelerometers, Measurement 24 (2) (September 1998) 87–96.
[4] T.-K. Kang, A simple four-point-bending setup for measurement of mechanical stress on silicon field-effect transistors, Measurement 44 (5) (2011) 871–874.
[5] P.S. André, H. Varum, P. Antunes, L. Ferreira, M.G. Sousa, Monitoring of the concrete curing process using plastic optical fibers, Measurement 45 (3) (2012) 556–560.
[6] P. Antunes, A.M. Rocha, H. Lima, H. Varum, P.S. André, Thin bonding wires temperature measurement using optical fiber sensors, Measurement 44 (3) (2011) 554–558.
[7] P. Antunes, H. Lima, H. Varum, P. André, Optical fiber sensors for static and dynamic health monitoring of civil engineering infrastructures: abode wall case study, Measurement 45 (7) (2012) 1695–1705.
[8] P. Antunes, H. Varum, P. André, Uniaxial fiber Bragg grating accelerometer system with temperature and cross axis insensitivity, Measurement 44 (1) (2011) 55–59.
[9] L. Wu, T. Cheng, Q.-C. Zhang, A bi-material microcantilever temperature sensor based on optical readout, Measurement 45 (7) (August 2012) 1801–1806.
[10] K.S. Karimov, F.A. Khalid, M.T.S. Chani, Carbon nanotubes based strain sensors, Measurement 45 (5) (2012) 918–921.
[11] A. Song, J. Wu, G. Qin, W. Huang, A novel self-decoupled four degree-of-freedom wrist force/torque sensor, Measurement 40 (9–10) (2007) 883–891.
[12] G. Rezazadeh, A. Lotfiani, S. Khalilarya, On the modeling of a MEMS-based capacitive wall shear stress sensor, Measurement 42 (2) (2009) 202–207.
[13] T. Sekitani, U. Zschieschang, H. Klauk, T. Someya, Flexible organic transistors and circuits with extreme bending stability, Nat. Mater. 9 (2010) 1015–1022.
[14] H. Tu, Y. Xu, A silicon-on-insulator complementary-metal-oxide-semiconductor compatible flexible electronics technology, Appl. Phys. Lett. 101 (5) (2012) 1–4. Paper 052106.
[15] D.-H. Kim, J. Xiao, J. Song, Y. Huang, J.A. Rogers, Stretchable, curvilinear electronics based on inorganic materials, Adv. Mater. 22 (19) (2010) 2108–2124.
[16] P.E. Burrows, G.L. Graff, M.E. Gross, P.M. Martin, M.K. Shi, M. Hall, E. Mast, C. Bonham, W. Bennet, M.B. Sullivan, Ultra barrier flexible substrates for flat panel displays, Displays 22 (2) (2001) 65–69.
[17] M.H. Godinho, H. Santos, A. Marques, V. Assunção, H. Águas, I. Ferreira, R. Martins, Surface modification of a new flexible substrate based on hydroxypropylcellulose for optoelectronic applications, Thin Solid Films 442 (1–2) (2003) 127–131.
[18] J.A. Rogers, T. Someya, H. Yonggang, Materials and mechanics for stretchable electronics, Science 327 (2010) 1603–1607.
[19] W.M. Choi, J. Song, D.-Y. Khang, H. Jiang, J.A. Rogers, Biaxially stretchable "wavy" silicon nanomembranes, Nano Lett. 7 (2007) 1655–1663.
[20] D.Y. Khang, H. Jiang, Y. Huang, J.A. Rogers, A stretchable form of single-crystal silicon for high-performance electronics on rubber substrates, Science 311 (2006) 208–212.
[21] H. Jiang, D.-Y. Khang, J. Song, Y. Sun, Y. Huang, J.A. Rogers, Finite deformation mechanics in buckled thin films on compliant supports, Proc. Natl. Acad. Sci. USA 104 (40) (2007) 15607–15612.
[22] S. Wang, J. Xiao, I. Jung, J. Song, H.C. Ko, M.P. Stoykovich, Y. Huang, K.-C. Hwang, J.A. Rogers, Mechanics of hemispherical electronics, Appl. Phys. Lett. 95 (18) (2009) 1–3. Paper 181912.
[23] A. Harb, Energy harvesting: state-of-the-art, Renew Energy 36 (10) (October 2011) 2641–2654.
[24] J.P. Carmo, M.F. Silva, J.F. Ribeiro, L.M. Gonçalves, J.H. Correia, Thermoelectric generator and solid-state battery for stand-alone microsystems, J. Micromech. Microengin. 20 (8) (2010) 1–8.
[25] H. Lhermet, C. Condemine, M. Plissonnier, R. Salot, P. Audebert, M. Rosset, Efficient power management circuit: from thermal energy harvesting to above-IC microbattery energy storage, IEEE J. Solid-State Circuits 43 (1) (2008) 246–255.
[26] R.-H. Kim, H. Tao, T.-I. Kim, Y. Zhang, S. Kim, B. Panilaitis, M. Yang, D.-H. Kim, Y. Hwan Jung, B.H. Kim, Y. Li, Y. Huang, F.G. Omenetto, J.A. Rogers, Materials and designs for wirelessly powered implantable light-emitting systems, Small 8 (18) (2012) 2812–2818.
[27] D.-H. Kim, N.Lu.Y. Huang, J.A. Rogers, Materials for stretchable electronics in bioinspired and biointegrated devices, MRS Bull. 37 (2012) 226–235.
[28] H. Kaase, J. Metzdorf, Photovoltaic solar cells: device parameters, calibration and applications, Measurement 4 (2) (1986) 28–42.
[29] R. Eke, A.S. Kavasoglu, N. Kavasoglu, Design and implementation of a low-cost multi-channel temperature measurement system for photovoltaic modules, Measurement 45 (6) (2012) 499–1509.
[30] M. Gagliarducci, D.A. Lampasi, L. Podestà, GSM-based monitoring and control of photovoltaic power generation, Measurement 40 (3) (2007) 314–321.
[31] G. Lenzi, V. Canevari, Solar cell test equipment, Measurement 11 (1) (1993) 33–37.
[32] Sylgard® 184 Silicone Elastomer, Dow Corning Corporation, <www.dowcorning.com>.
[33] J.C. Lötters, W. Olthuis, P.H. Veltink, P. Bergveld, The mechanical properties of the rubber elastic polymer polydimethysiloxane for sensor applications, J. Micromechan. Microengin. 7 (1997) 145–147.
[34] B.-H. Jo, Three-dimensional micro-channel fabrication in polydimethylsiloxane (PDMS) elastomer, IEEE J. Microelectromech. Syst. 9 (1) (2000) 76–81.
[35] M. Liu, J. Sun, Q. Chen, Influences of heating temperature on mechanical properties of polydimethylsiloxane, Sensors and Actuators A: Physical 151 (1) (2009) 42–45.

[36] Pyralux® Flexible Circuit Materials, DuPont. <www.dupont.com>.
[37] Ultrathin rechargeable lithium polymer batteries, PowerStream Technology, <www.powerstream.com>.
[38] Foldable Solar Panels, PowerFilm Solar Inc. <www.powerfilmsolar.com>.
[39] Linear Technology Corporation, <www.linear.com>.
[40] R. Morais, M.A. Fernandes, S.G. Matos, C. Serôdio, P.J.S.G. Ferreira, M.J.C.S. Reis, A ZigBee multi-powered wireless acquisition device for remote sensing applications in precision viticulture, Comput. Electron. Agric. 62 (2008) 94–106.
[41] R. Morais, S.G. Matos, M.A. Fernandes, A.L.G. Valente, S.F.S.P. Soares, P.J.S.G. Ferreira, M.J.C.S.Reis, Sun, wind and water flow as energy supply for small stationary data acquisition platforms, Comput. Electron. Agric. 64 (2008) 120–132.